Front. Phys. 11(6), 114207 (2016)
DOI 10.1007/s11467-016-0592-3

RESEARCH ARTICLE

Preliminary investigation into feasibility of dissolved methane measurement using cavity ringdown spectroscopy technique

Zhen-Nan Wang (王振南), **Wang-Quan Ye** (叶旺全), **Xiao-Ning Luan** (栾晓宁), **Fu-Jun Qi** (亓夫军), **Kai Cheng** (程凯), **Ronger Zheng** (郑荣儿)†

Optics and Optoelectronics Laboratory, Ocean University of China, Qingdao 266100, China
Corresponding author. E-mail: †rzheng@ouc.edu.cn
Received January 24, 2016; accepted April 30, 2016

For the exploration of gas hydrate resources by measuring the dissolved methane concentration in seawater, a continuous-wave cavity ringdown spectroscopy (CW-CRDS) experimental setup was constructed for trace methane detection. A current-modulation method, rather than a cavity-modulation method using an optical switch and a piezoelectric transducer, was employed to realize the cavity excitation and shutoff. Such a current-modulation method enabled the improvement of the experimental setup construction and stability, and the system size and stability are critical for a sensor to be deployed underwater. Ringdown data acquisition and processing were performed, followed by an evaluation of the experimental setup stability and sensitivity. The obtained results demonstrate that great errors are introduced when a large fitting window is selected if the analog-to-digital converter has an insufficient resolution. The ringdown spectrum of methane corresponding to the $2\nu_3$ band R(4) branch was captured, and the methane concentration in lab air was determined to be 2.06 ppm. Further experiments for evaluating the quantitative ability of this CW-CRDS experimental setup are underway from which a high-sensitivity methane sensor that can be combined with a degassing system is expected.

Keywords gas hydrate, methane, continuous-wave cavity ringdown spectroscopy, current-modulation method

PACS numbers 42.62.Fi, 91.50.Hc

1 Introduction

The bottom-simulating reflector (BSR), which is a seismic reflection at the sediment interface caused by the unequal densities of normal and gas hydrate-bearing sediments, is well-known as a principal indicator of the marine gas-hydrate zone [1, 2]. However, it is neither a necessary nor sufficient condition. Gas hydrate has been found where there is no BSR [3, 4]. Abnormally high methane concentrations have been observed in the water column above the gas-hydrate zone and hydrothermal vent field [5–10]; therefore, the observation of a methane plume is a potential indicator of gas hydrate and a hydrothermal vent. However, the background methane concentration in the seawater is as low as a few nanomoles per liter (nmol/L) level [11–14], which requires measurement instrumentations and sensors with high sensitivity. In general, the most widely used technique is gas chromatography (GC). Dissolved methane in seawater is first extracted using a stripping/trapping system and then measured by a gas chromatograph in the laboratory or onboard. Although it has high sensitivity and selectivity, GC is not suitable for real-time or in-situ measurement, because of its time-consuming sample preparation and processing procedure.

Cavity ringdown spectroscopy (CRDS) is a newly developed laser absorption technique with high sensitivity, high selectivity, rapid response, and the capability of absolute quantification [15, 16], and its application for trace methane measurement has been reported [17–19]. Wang *et al.* developed a standalone continuous-wave (CW) cavity ringdown spectrometer for the in-situ measurement of methane, carbon dioxide, and carbon-

Frontiers of Physics

dioxide isotopes [20]. The detection limit of 0.2 parts per million (ppm) methane and 120 ppm carbon dioxide were obtained at atmospheric pressure.

Commercial CRDS instruments are also available for methane detection in atmospheric air. Crosson developed a field-deployable cavity ringdown analyzer for the measurement of the atmospheric levels of carbon dioxide, methane, and water vapor [21]. A field test using a methane gas bottle demonstrated that this CRDS analyzer had a precision of 0.5 ppb (parts per billion) in a 5s measurement and a peak-to-peak drift of 0.8 ppb over an 18-day period. After the Deepwater Horizon oil spill in the Gulf of Mexico in 2010, Yvon-Lewis *et al.* measured the methane concentration in air and seawater using a cavity ringdown spectrometer and a gas chromatograph for the investigation of the sea-to-air methane flux [22]. The methane in the air was analyzed directly, whereas that dissolved in the seawater was extracted using a continuously flowing seawater equilibrium. For continuously measuring the methane and carbon dioxide concentrations in the surface water of the Baltic Sea, Gülzow *et al.* installed an analytical setup that consisted of a methane/carbon dioxide analyzer (MCA, based on off-axis integrated cavity output spectroscopy, a variant of CRDS) and a bubble-type equilibrator on a cargo ship [23]. The obtained results demonstrated that the methane concentrations measured by GC and by the MCA agreed well. No such CRDS system has been deployed underwater for dissolved methane measurement.

In the present study, with the hope of developing a trace methane sensor for dissolved methane measurement that can be combined with a degassing system, a CW-CRDS experimental setup was constructed using a current-modulation method. The design scheme of the CW-CRDS setup is introduced, along with detailed illustrations of its control and operation. The methane concentration in lab air was measured by scanning the ringdown spectrum of methane at 1650.96 nm.

2 Experimental

2.1 Experimental setup

A schematic of the CW-CRDS experimental setup is shown in Fig. 1. A tunable distributed feedback laser diode (DFB-LD, NTT Electronics, NLK1U5FAAA) in a butterfly-type 14-pin package was employed as a light source and was mounted on an LD mounting fixture (ILX Lightwave, LDM-4980). An LD controller (ILX Lightwave, LDC-3724C), which is an instrument comprising an LD current driver and a temperature controller, was connected to the LD mount fixture to control the LD forward current and operating temperature. The pigtail

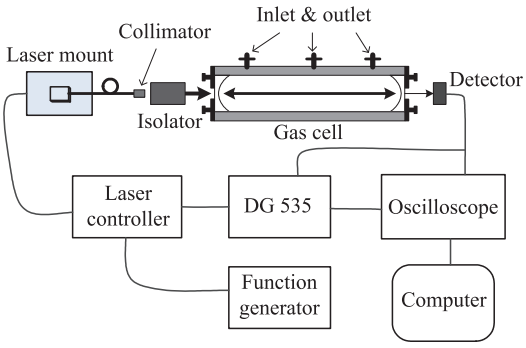

Fig. 1 Schematic of the CW-CRDS experimental setup.

fiber of the LD was connected to a micro-telescope so that the output laser beam was collimated before being injected into a gas cell (CRD Optics). An optical isolator (Thorlabs) was placed between the micro-telescope and the gas cell to prevent optical feedback into the laser source.

The gas cell was a ringdown cavity comprising a 500-mm-long stainless steel pipe with an inner diameter of 30 mm, a pair of mirror mounts, and a pair of high-reflectivity mirrors. The mirrors had a reflectivity of >99.99% at 1650 nm and a radius of curvature of 1,000 mm. Each mirror was held by a mirror mount and adjusted in multiple dimensions via the three alignment screws of the mirror mount. The gas cell had three ports that functioned as the gas sample inlet and outlet. A switchable gain photodetector (Thorlabs, PDA10CS-EC) was placed behind the rear mirror to detect the ringdown signal, and an oscilloscope (Tektronix, TDS1002B) was used to monitor the ringdown waveform and convert the analog ringdown signal into digital data that were transmitted to a computer for analysis.

To realize the cavity excitation and shutoff in this CW-CRDS setup, a current-modulation method was applied, rather than using an acousto-optic modulator and piezoelectric transducer. The LD controller used in this setup supported external current modulation up to 1MHz. A direct-current (DC) signal from a digital delay/pulse generator (DDG, Stanford Research Systems, DG535) and a triangular wave generated by a function signal generator (Nanjing Xinlian Telecommunication Instruments Company, EE1641D) were fed to the LD current driver as external modulation signals through a power combiner. The DC signal from the DDG served as the primary source of the LD forward current to drive the LD, and the triangular wave was used to modulate the laser output wavelength. The laser frequency varied with the modulation of the triangular wave, and the laser beam was coupled into the ringdown cavity and excited it once the laser frequency matched the resonant frequency of the cavity. Subsequently, to observe the cavity ringdown

waveform, the DC signal from the DDG was shut down so that the laser output was cut off.

2.2 Experimental control and operation

As described in the previous section, a current-modulation method was applied to realize cavity excitation and shutoff. A detailed experimental control procedure is introduced in this section. The LD response characteristics were tested to demonstrate the feasibility of the current-modulation method.

Figure 2 summarizes the procedure for the cavity excitation and shutoff. In general, the LD driving current from the LD driver, along with the DDG pulsed voltage, and the triangular wave were combined to drive the LD. The LD driving current generated by the LD driver [Fig. 2(a)] was lower than the LD threshold current (20 mA); thus, the LD had no output in this case. The low driving current from the LD driver was used to prevent the LD from undergoing absolute shutdown when the voltage signal from the DDG decreased to zero. According to the cavity length of 500 mm and the LD current-modulation rate of 0.010 nm/mA, the amplitude of the triangular wave [Fig. 2(b)] was determined to be 14 mV to ensure that the variation of the laser output frequency covered at least one free spectral range (FSR) of the cavity, i.e., 300 MHz. In the experiment, this value was set at ~20 mV so that the laser frequency variation covered 1.5 FSR. The triangular-wave frequency was set at 10 Hz. The pulsed voltage signal [Fig. 2(c)] generated by the DDG was used to provide a driving current to the LD, and the LD forward current reached 120 mA when the high level of the DDG signal was ~2.0 V along with the contribution of LD driving current and triangular wave. Under the modulation of the triangular wave, the

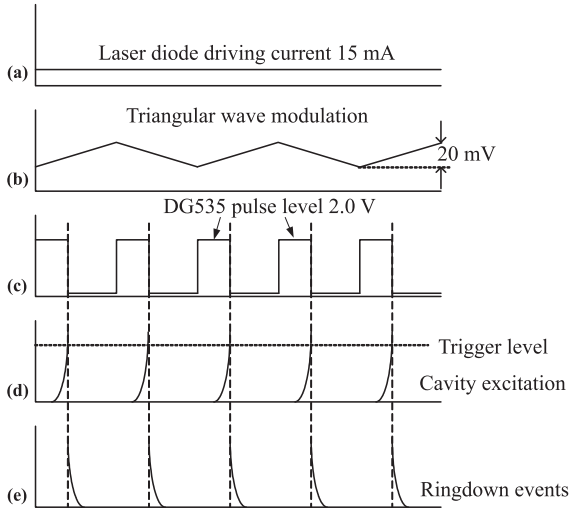

Fig. 2 Procedure for cavity excitation and shutoff.

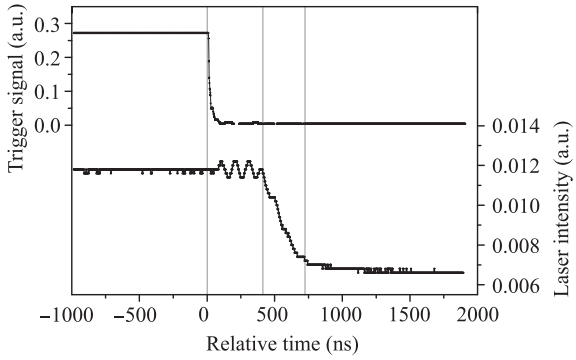

Fig. 3 System insert delay and LD response to cavity shutoff signal.

laser beam was coupled into the cavity regularly. Once the signal intensity detected by the detector reached a set trigger level [Fig. 2(d)] (i.e., 1 V), the DDG shut down its DC output, as shown in Fig. 2(c), and the laser output was shut off soon afterward. Simultaneously, a synchronizing signal generated by the DDG was used to trigger the oscilloscope to capture the ringdown signal decay [Fig. 2(e)]. The low-level (0 V) duration of the DDG pulse was set to 1 ms to ensure that the ringdown decay was completed.

To demonstrate the feasibility of the current-modulation method, the system insert delay and LD response were tested. Figure 3 shows the system insert delay and the LD response to the cavity shutoff signal. Channel 2 waveform was a synchronizing signal whose falling edge was used to trigger the oscilloscope for capturing a ringdown signal. The laser intensity of channel 1 waveform was monitored by the detector. As shown in Fig. 3, ~400 ns after the DDG was triggered, the laser intensity began to decrease and shut down in ~300 ns, which was far less than the ringdown time (~20 μs).

3 Results and discussion

3.1 Ringdown decay acquisition and processing

Figure 4 shows the typical ringdown waveforms displayed on the oscilloscope. The rising edge of each waveform indicates the cavity excitation process, and the falling edge shows the exponential ringdown decay. The rising edges are unsmooth, which indicates that the noise in the driving and modulation current affected the realization of the cavity excitation.

To determine the ringdown time, a logarithm operation was applied to the ringdown decay waveform, followed by fitting it to a linear regression, and the ringdown time was obtained by taking the reciprocal value of the fitted line slope. Figure 5 shows the ringdown

time determination using this method. Figures 5(a) and (c) show the ringdown data in the ranges of 3–23 and 3–43 μs, respectively, and Figs. 5(b) and (d) show the linear fitting results. The ringdown times were determined to be 20.84 and 20.31 μs, respectively. The obtained ringdown times were close, although different fitting windows were selected. However, the lower panels in Figs. 5(b) and (d) indicate that the fitting residual was greater when the fitting window was larger. This suggests that large errors might be introduced in the linear fitting process if a large fitting window is used.

To investigate the possible error introduced by a large fitting window, the ringdown waveform data at the end of the fitting window (i.e., 33–43 μs) were selected for fur-

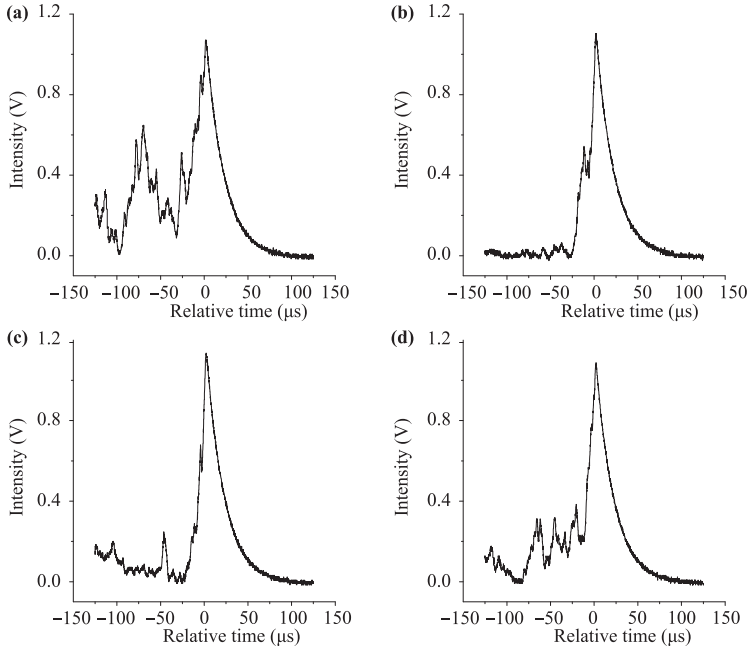

Fig. 4 Typical ringdown waveforms captured by the oscilloscope.

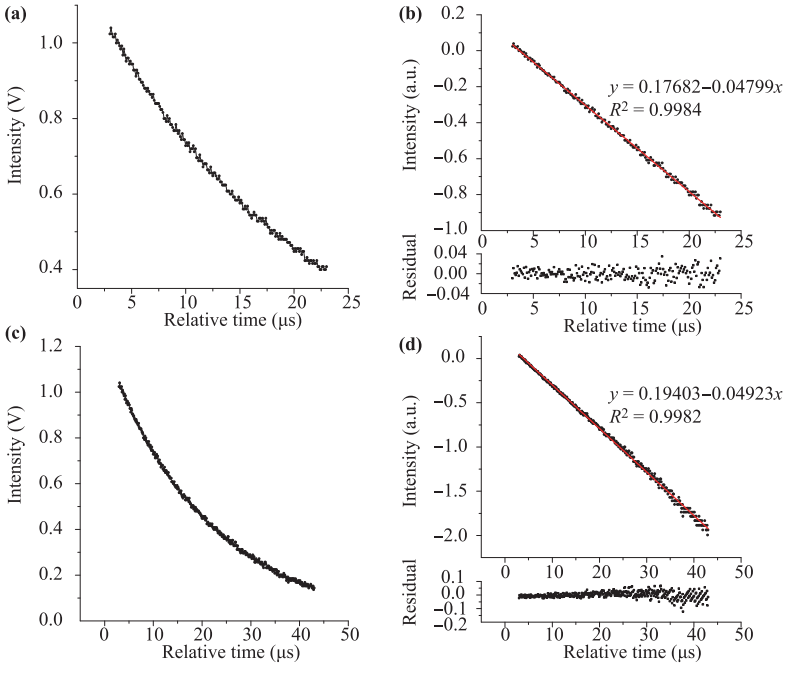

Fig. 5 Ringdown time determination by fitting a linear regression to the logarithm of the ringdown waveform.

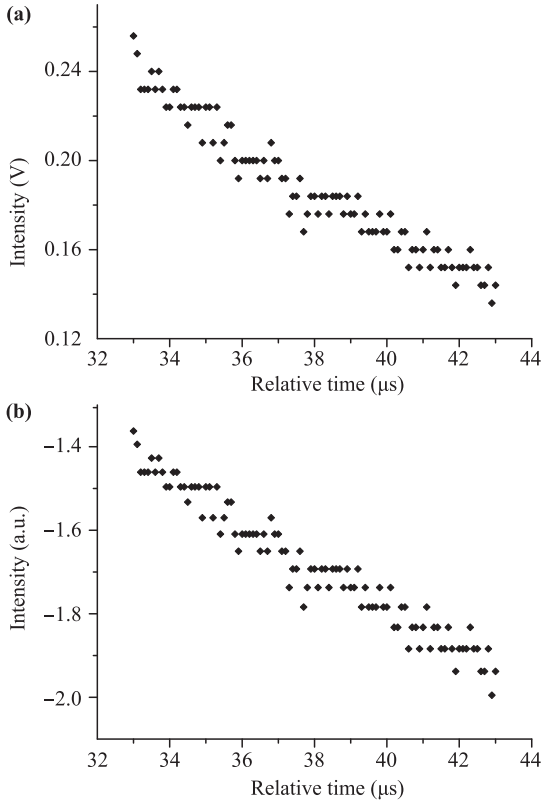

Fig. 6 Ringdown waveform data at the end of a larger fitting window: 33–43 μs.

ther analysis, as shown in Fig. 6. Figure 6(a) shows the originally captured ringdown data, and Fig. 6(b) shows the corresponding data after the implementation of the logarithm operation. The ringdown signals decreased with time; however, many data points at different times had the same intensity value. This phenomenon demonstrates that the analog-to-digital convertor (ADC), i.e., the oscilloscope in this experimental setup, could not distinguish adjacent data points, owing to its limited 8 bit resolution. This result suggests that the selected fitting window should be restricted in the case of an ADC with a low resolution.

3.2 System stability and sensitivity

After the CW-CRDS experimental setup was constructed, several tests were conducted to check its stability and sensitivity. The ringdown time baseline stability was defined as $\sigma/\bar{\tau}$, where σ and $\bar{\tau}$ are the standard deviation (SD) and mean value of the ringdown time, respectively. Figure 7 shows the ringdown time stability in terms of the ringdown time for various average numbers and fitting windows. In Fig. 7(a), each data point represents the ringdown time obtained by averaging 16 ringdown events and selecting the fitting window of 3–23 μs, and the x-axis represents the number of data points. Figures 7(a)–(c) show the ringdown time obtained with the same fitting window but different average numbers of ringdown events. Figures 7(d)–(i) can be deduced by analogy.

Table 1 Ringdown time obtained with various average numbers and fitting windows.

Fitting window (μs)	Average number	Mean (μs)	SD (μs)	RSD (%)
3–23	16	20.53	0.14	0.70
	64	20.44	0.11	0.55
	128	20.47	0.08	0.37
3–33	16	20.38	0.18	0.90
	64	20.27	0.14	0.67
	128	20.28	0.09	0.43
3–43	16	20.41	0.24	1.15
	64	20.27	0.18	0.87
	128	20.28	0.11	0.56

SD: Standard deviation; RSD: Relative standard deviation.

The average numbers of ringdown events were selected to be 16, 64, and 128. The fitting windows were 3–23, 3–33, and 3–43 μs, corresponding to 1, 1.5, and 2 times the ringdown time, respectively. Table 1 lists the obtained results in terms of the mean ringdown time, SD, and relative SD (RSD). For each fitting window, there is no doubt that the RSD of the ringdown time tended to decrease with the increase in the average number of ringdown events. With each determined ringdown event average number, the obtained results indicate that the RSD of ringdown time tended to increase with the fitting window. A possible reason for this was previously explained: the insufficient vertical resolution of the oscilloscope.

The ringdown time baseline stability was as good as 0.37% for a ringdown time average number of 128 and a fitting window of 3–23 μs. Using a mirror reflectivity of 99.993% at 1,650 nm, a cavity length of 500 mm, and a methane absorption cross-section of 1.87×10^{-20} cm^2/molecule, the limit of detection of methane was determined to be ∼31 ppb (parts per billion) according to the standard 3-σ criterion [20].

3.3 Methane measurements

Methane in the atmospheric air, whose concentration is ∼1.8 ppm on average [24], was measured using the CW-CRDS experimental setup. Figure 8 shows the typical ringdown spectrum of methane near 1650.96 nm, which corresponds to the $2\nu_3$ band R(4) branch and was obtained by scanning the LD temperature from 25 to 29 °C with steps of 0.1 °C. The top x-axis represents the LD emission wavelength in nanometers, which was calculated using a methane $2\nu_3$ band R(4) branch of 1,650.96

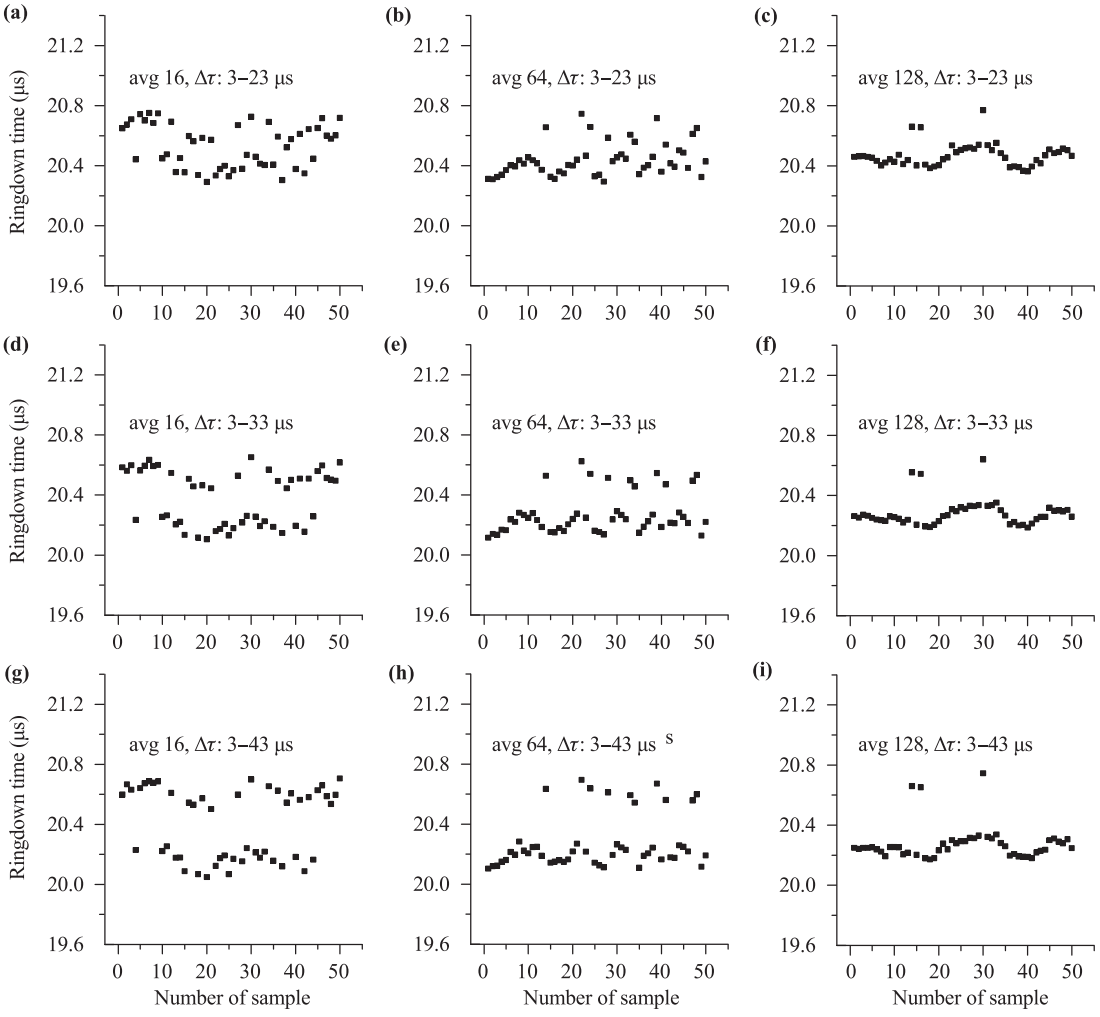

Fig. 7 Ringdown baseline stability in terms of the ringdown time with different average numbers and fitting windows.

nm, an LD temperature tuning rate of ~0.1 nm/°C, and a tuning step of 0.1 °C. Each data point in Fig. 8 was obtained by averaging 128 ringdown events and using a fitting window of 3–23 μs, an LD forward current of 120 mA, and a triangular wave with a frequency of 10 Hz and amplitude of 10 mV. As the LD temperature tuning rate was ~0.1 nm/°C, the variation of the laser output wavelength was ~0.4 nm. This experiment was performed at room temperature and atmospheric pressure. The methane concentration was determined using the following equation:

$$\text{Absorbance} = \sigma(\lambda)nd = d(1/\tau - 1/\tau_0)/c, \quad (1)$$

where $\sigma(\lambda)$ is the methane absorbance cross section at 1650.96 nm; n is the methane concentration; d is the cavity length; c is the speed of light; and τ and τ_0 are the ringdown times when the laser was tuned on and off the line, respectively. Letting the ringdown times when the LD temperature was 26.5 and 27.2 °C be τ and τ_0, respectively, the measured concentration of methane was 2.06 ppm.

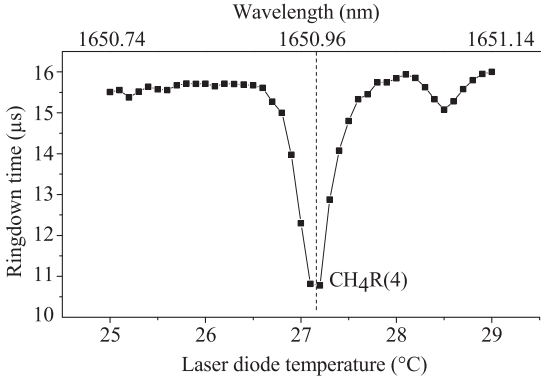

Fig. 8 Typical ringdown spectrum of methane in the atmospheric air.

4 Conclusions

A CW-CRDS experimental setup was constructed and evaluated in terms of the stability and sensitivity for measuring methane. A current-modulation method was used to realize the cavity excitation and shutoff. In general, a triangular wave was applied to modulate the laser output wavelength so that the laser beam could be coupled into the resonant cavity to excite the cavity once its frequency matched the resonant frequency of the ringdown cavity. The LD forward current was shut down subsequently to shutting off the laser output; consequently, the ringdown-decay waveform was observed. More details about the experimental control and operation procedure were introduced. Such a current-modulation method makes the improvement of the experimental-setup construction and stability possible. The ringdown time was obtained by running a logarithm operation to the ringdown waveform and then fitting it to a linear regression. A significant error was introduced if a large fitting window was chosen when the ADC had an insufficient resolution. The ringdown spectrum of methane corresponding to the $2\nu_3$ band R(4) branch was measured, and the methane concentration in lab air was determined to be 2.06 ppm. Further experiments for evaluating the quantitative ability of this CW-CRDS experimental setup are underway. A high-sensitivity methane sensor that can be combined with a degassing system is expected.

Acknowledgements The work was partially supported by the Fundamental Research Funds for the Central Universities and the National High Technology Research and Development Program of China (Grant No. 2012AA09A405). The author Zhennan Wang thanks Dr. Chuji Wang for very valuable discussions on the experimental setup.

References

1. R. D. Hyndman and G. D. Spence, A seismic study of methane hydrate marine bottom simulating reflectors, *J. Geophys. Res.* 97(B5), 6683 (1992)
2. R. D. Hyndman and E. E. Davis, A mechanism for the formation of methane hydrate and seafloor bottom-simulating reflectors by vertical fluid expulsion, *J. Geophys. Res.* 97(B5), 7025 (1992)
3. W. S. Holbrook, H. Hoskins, W. T. Wood, R. A. Stephen, and D. Lizarralde, Methane hydrate and free gas on the Blake Ridge from vertical seismic profiling, *Science* 273(5283), 1840 (1996)
4. J. Yuan and R. N. Edwards, The assessment of marine gas hydrates through electrical remote sounding: Hydrate without a BSR? *Geophys. Res. Lett.* 27(16), 2397 (2000)
5. T. F. Yang, P. C. Chuang, S. Lin, J. C. Chen, Y. Wang, and S. H. Chung, Methane venting in gas hydrate potential area offshore of SW Taiwan: evidence of gas analysis of water column samples, *Terr. Atmos. Ocean. Sci.* 17, 933 (2006)
6. C. K. Paull, W. Ussler, W. S. Borowski, and F. N. Spiess, Methane-rich plumes on the Carolina continental rise: Associations with gas hydrates, *Geology* 23(1), 89 (1995)
7. C. A. Chen, Abnormally high CH_4 concentrations in seawater at mid-depths on the continental slopes of the northern South China Sea, *Terr. Atmos. Ocean. Sci.* 17, 951 (2006)
8. Y. Zhang, Methane escape from gas hydrate systems in marine environment, and methane-driven oceanic eruptions, *Geophys. Res. Lett.* 30(7), 1398 (2003)
9. H. Zhou, Z. Wu, X. Peng, L. Jiang, and S. Tang, Detection of methane plumes in the water column of Logatchev hydrothermal vent field, Mid-Atlantic Ridge, *Chin. Sci. Bull.* 52(15), 2140 (2007)
10. E. J. Sauter, S. I. Muyakshin, J. L. Charlou, M. Schlüter, A. Boetius, K. Jerosch, E. Damm, J. P. Foucher, and M. Klages, Methane discharge from a deep-sea submarine mud volcano into the upper water column by gas hydrate-coated methane bubbles, *Earth Planet. Sci. Lett.* 243(3-4), 354 (2006)
11. S. Watanabe, N. Higashitani, N. Tsurushima, and S. Tsunogai, Methane in the western North Pacific, *J. Oceanogr.* 51(1), 39 (1995)
12. H. W. Bange, U. H. Bartell, S. Rapsomanikis, and M. O. Andreae, Methane in the Baltic and North Seas and a reassessment of the marine emissions of methane, *Global Biogeochem. Cycles* 8(4), 465 (1994)
13. N. J. P. Owens, C. S. Law, R. F. C. Mantoura, P. H. Burkill, and C. A. Llewellyn, Methane flux to the atmosphere from the Arabian Sea, *Nature* 354(6351), 293 (1991)
14. B. D. Tilbrook and D. M. Karl, Methane sources, distributions and sinks from California coastal waters to the oligotrophic North Pacific gyre, *Mar. Chem.* 49(1), 51 (1995)
15. A. O'Keefe and D. A. G. Deacon, Cavity ring-down optical spectrometer for absorption measurements using pulsed laser sources, *Rev. Sci. Instrum.* 59(12), 2544 (1988)
16. D. Romanini, A. A. Kachanov, N. Sadeghi, and F. Stoeckel, CW cavity ring down spectroscopy, *Chem. Phys. Lett.* 264(3–4), 316 (1997)
17. B. L. Fawcett, A. M. Parkes, D. E. Shallcross, and A. J. Orr-Ewing, Trace detection of methane using continuous wave cavity ring-down spectroscopy at 1.65 μm, *Phys. Chem. Chem. Phys.* 4(24), 5960 (2002)
18. M. Hippler and M. Quack, High-resolution Fourier transform infrared and cw-diode laser cavity ringdown spectroscopy of the $\nu_2+2\nu_3$ band of methane near 7510 cm^{-1} in slit jet expansions and at room temperature, *J. Chem. Phys.* 116(14), 6045 (2002)

19. J. J. Scherer, D. Voelkel, D. J. Rakestraw, J. B. Paul, C. P. Collier, R. J. Saykally, and A. O'Keefe, Infrared cavity ringdown laser absorption spectroscopy (IR-CRLAS), *Chem. Phys. Lett.* 245(2–3), 273 (1995)

20. C. Wang, N. Srivastava, B. A. Jones, and R. B. Reese, A novel multiple species ringdown spectrometer for in situ measurements of methane, carbon dioxide, and carbon isotope, *Appl. Phys. B* 92(2), 259 (2008)

21. E. R. Crosson, A cavity ring-down analyzer for measuring atmospheric levels of methane, carbon dioxide, and water vapor, *Appl. Phys. B* 92(3), 403 (2008)

22. S. A. Yvon-Lewis, L. Hu, J. D. Kessler, F. Garcia Tigreros, E. W. Chan, and M. Du, Methane flux to the atmosphere from the Deepwater Horizon oil leak, *AGU Fall Meet. Abstr.* 1, 06 (2010)

23. W. Gülzow, G. Rehder, B. Schneider, J. S. V. Deimling, and B. Sadkowiak, Limnol. A new method for continuous measurement of methane and carbon dioxide in surface waters using off-axis integrated cavity output spectroscopy (ICOS): An example from the Baltic Sea, Oceanogr, *Methods* 9, 176 (2011)

24. M. Heimann, Atmospheric science: Enigma of the recent methane budget, *Nature* 476(7359), 157 (2011)